Article

Online plasma measurement using the TJ-II FPGA-based IR interferometer

Luis Esteban [1] and Alberto Regadío [2]

[1] ARIES Research Center, Universidad Antonio Nebrija, Madrid, Spain; lesteban@nebrija.es
[2] Instituto Nacional de Técnica Aeroespacial (INTA), Madrid, Spain; regadioca@inta.es

Abstract: Interferometry is used in magnetic fusion devices to measure the line-averaged electron density. It is based on detecting changes in the refractive index of electromagnetic waves traveling through a plasma. The adequate frequency of these electromagnetic waves depends on several limitations. First the maximum expected peak electronic density must be lower than the cutoff density for that frequency. This means that the waves can still propagate through the plasma when the maximum density is reached. In this sense, IR interferometers operating in the infrared region are the most suitable. With such low wavelengths, mechanical vibrations become an important issue and a complementary interferometer to cancel these vibrations must be used. These arrangements are called two color interferometers. In this paper some measurements that were obtained from the TJ-II double color IR FPGA-based processing system that were never published before are shown and analyzed. **The line-averaged electron density is computed in real time (**100 μs**).**

Keywords: Magnetic fusion devices; IR interferometry; FPGA; phase detection; DSP

1. Introduction

In the beginning of the fifties, the research and development of nuclear fusion was launched, with the aim of obtaining energy in a cleaner, more reliable and long lasting way. The easiest fusion reaction takes place between Deuterium (D) and Tritium (T) to produce Helium (He) and energy. This reaction takes place if the mutual repulsion forces that exists between the two nuclei are balanced. A way of making this possible is to increase the temperature to values higher than 10^7 ºC, in which the fuel (D and T) is completely ionized and in the plasma state. With such a high temperature the plasma must be kept separate from its material container, otherwise the plasma will be quickly cooled and severe damage to the container walls might occur. Taking advantage of the fact that the plasma consists of charged particles, one way to do this is by magnetic confinement. Under this concept two type of devices arise, the tokamak [1] and the stellarator [2].

Due to the inherent complexity of magnetic confinement it is essential to measure the properties of the plasma with the highest accuracy possible. Several measuring methodologies have been developed around magnetic fusion devices. An important group of these methodologies are based on the measure of the change of the refractive index suffered by electromagnetic waves that cross the plasma.

TJ-II plasmas are cold magnetized ones, where the thermal speed of electrons is much lower than that of light $v_e \ll c$. The refractive index is [3]:

$$N = \sqrt{1 - \frac{\omega_p^2}{\omega^2}}, \tag{1}$$

ω_p is the plasma frequency given by:

$$\omega_p^2 = \frac{n_e e^2}{\varepsilon_0 m_e} + \frac{n_i e^2}{\varepsilon_0 m_i}, \tag{2}$$

m_e and m_i are the mass of the electron and the ion respectively and n_e and n_i their densities. Since $m_i \simeq 1600 \cdot m_e$ it can be concluded that electron density governs the properties of the refractive index:

$$\omega_p^2 \simeq \frac{n_e e^2}{\varepsilon_0 m_e}. \tag{3}$$

The line-integrated plasma density can be calculated according to the Appleton-Hartree relation [4–6]. Interferometers are devices used for these types of measurements [7–13], choosing the wavelength of the radiation according to the density range that is going to be measured.

Interferometers operating in the medium infrared (IR) range are suitable for measuring high electron densities. These systems usually use heterodyne modulation [14] and are equipped with a second wavelength (color) to correct low frequency mechanical vibrations and thermal drifts.

Essentially, these devices measure optical path length variations and these variations are proportional to the line-integrated electron density, which can be expressed as:

$$\int_0^L n_e(z)\mathrm{d}z, \tag{4}$$

where L is the integration path across the plasma or chord-length. Estimating the value of L, the average density is evaluated as:

$$< n_e >= \frac{\int_0^L n_e(z)\mathrm{d}z}{L}. \tag{5}$$

For higher electron densities and for a given wavelength above a certain value of the electron density the plasma becomes reflective (cut-off density) [6]. Therefore, shorter wavelengths will allow the measurement of higher electron densities. On the other hand the shorter the wavelengths are the more sensitive the interferometer is to mechanical vibrations and thermal drifts. For interferometers operating in the Far Infrared (FIR) and in the Middle Infrared (MIR) regions it is necessary to use another interferometer with a different wavelength to compensate these mechanical vibrations. These devices are called two color or two wavelength interferometers. The optical path length of one of the interferometers will vary because of plasma density variations and mechanical vibrations and the optical path length of the other one will vary mainly because of mechanical vibrations.

The phase shift of the beam crossing a plasma is given by:

$$\Delta\phi = \frac{\pi}{\lambda n_{co}} \int_0^L n(z)\mathrm{d}z, \tag{6}$$

where L is the integration path across the plasma, $n_{co} = \varepsilon_0 m_e \left(2\pi f/e\right)$ is the cutoff electron density and f is the probing frequency. The total phase shift will not only be caused by plasma density fluctuations but also because of changes in the optical paths:

$$\Delta\phi = \frac{\lambda}{r_e} \int_0^L n(z)\mathrm{d}z + 2\pi\frac{\Delta l}{\lambda}, \tag{7}$$

r_e is the classical electron radius. If two wavelengths are used, both optical paths can be expressed as:

$$\Delta\phi_1 = \frac{\lambda_1}{r_e} \int_0^L n(z)\mathrm{d}z + 2\pi\frac{\Delta l}{\lambda_1}, \tag{8}$$

$$\Delta\phi_2 = \frac{\lambda_2}{r_e} \int_0^L n(z)\mathrm{d}z + 2\pi\frac{\Delta l}{\lambda_2}. \tag{9}$$

If both sides of Eq. 8 are multiplied by λ_1 and both sides of Eq. 9 by λ_2 we can obtain the electron density by subtracting both equations and canceling the term $2\pi\Delta l$ and by hence the mechanical vibrations. The final expression for the electron density is given by:

$$\int n_e \mathrm{d}l = \frac{\Delta\phi_1\lambda_1 - \Delta\phi_2\lambda_2}{\mathrm{r_e}(\lambda_1^2 - \lambda_2^2)}. \tag{10}$$

If the probing beams cross the plasma p times, the final line-integrated density is evaluated as:

$$\int n_e \mathrm{d}l = \frac{\Delta\phi_1\lambda_1 - \Delta\phi_2\lambda_2}{p \cdot \mathrm{r_e}(\lambda_1^2 - \lambda_2^2)}, \tag{11}$$

the difference, $(\Delta\phi_1\lambda_1 - \Delta\phi_2\lambda_2)$ is the compensated optical path length.

In the TJ-II Stellarator a double color CO_2 $(10.591\ \mu\mathrm{m}) - \mathrm{Nd:YAG}$ $(1.064\ \mu\mathrm{m})$ interferometer has been routinely used to measure higher electron plasma densities, first using an off-line slower processing system [9] and later by using an online Field Programmable Gate Array (FPGA) based processing system [15–17]. The interferometer setup is shown on Figure 1. The devices labeled AOM1 and AOM2 are Acousto-Optic-Modulators used to generate heterodyne frequencies. They split the incoming beams into two beams, reference and probing, and in the latter they also introduce a frequency displacement fixed by a local oscillator $(40\ \mathrm{MHz})$. Mirror M_{12} is used to launch the probing beams into the plasma and also to send the reflecting beams backwards to the detectors. Once the probing and reference beams reach the detectors they interfere generating two interference signals with frequencies equal to those introduced by the AOMs. By measuring the phase shift suffered by the probing signals the line-averaged electron density can be calculated.

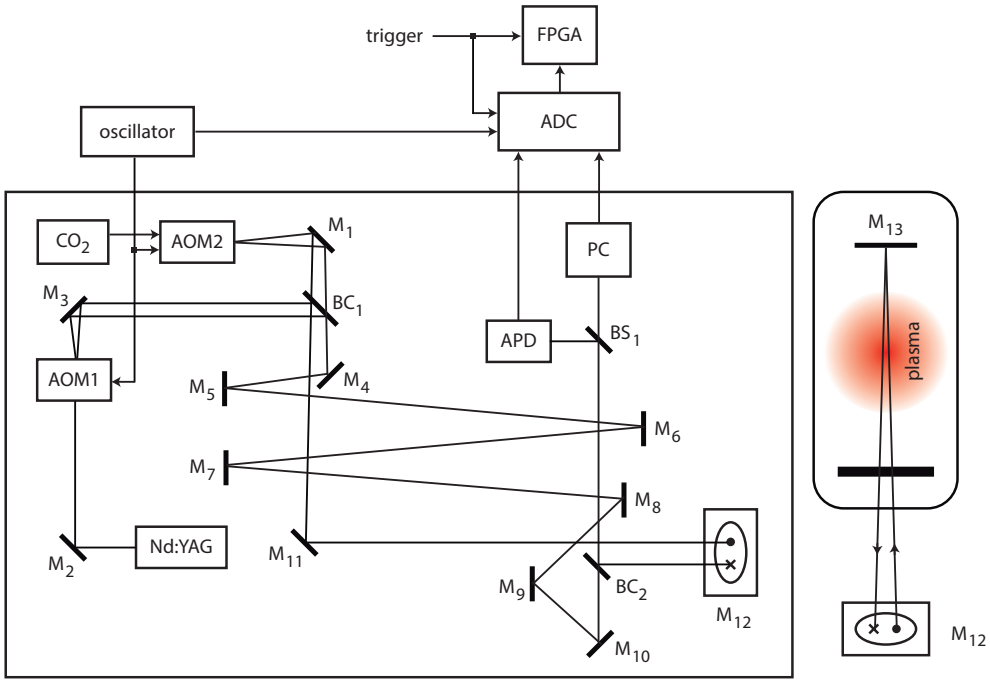

Figure 1. Detail of the two color IR infrared interferometer including the FPGA-based backend electronics.

This paper is structured as follows: Section 2 reviews how the phase measurements in the TJ-II IR interferometer are done. Section 3 shows results obtained with this FPGA-based backend in static conditions and during normal operation of the TJ-II device and finally, in Section 4 the main conclusions of this work are summarized.

2. Phase measurement

The computation of the line-electron density given by Eq. 11 requires proper measurement of the phase shifts of the interference signals, $\Delta\phi_1$ and $\Delta\phi_2$. In the case of interferometers operating in the middle infrared range, the modulation frequencies are in the order of tens of MHz. These values are fixed because of physical constraints of the Acousto-Optical-Modulators (AOMs) used to generate the heterodyne frequencies. In the past due to the limitations of the processing systems, it was necessary to use analog frequency mixing stages as the one shown in Figure 2.

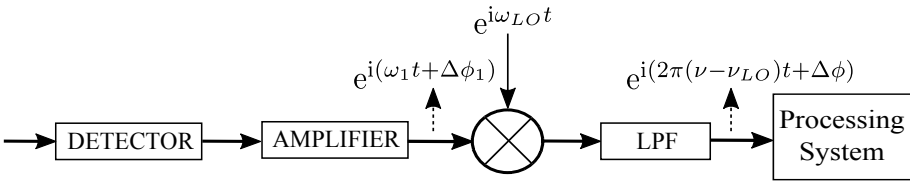

Figure 2. Scheme of the analog frequency mixing stage. The interference signal is detected, amplified, mixed to a lower frequency and filtered to remove the high frequency component.

For instance, initially in the TJ-II IR interferometer, after detecting the inteference signal, with frequency ν, it was mixed with another signal synthesized in a local oscillator, ν_{LO}. The mixing procedure resulted in a signal having two main frequency components, $\nu - \nu_{LO}$ and $\nu + \nu_{LO}$. The high frequency one was removed using a low pass filter and an output with a lower manageable frequency, $\nu - \nu_{LO}$ was obtained. This signal was equivalent in amplitude and phase response to the original detected interference signal. In the case of the TJ-II interferometer the subsequent signal processing was performed by a digital off-line Analog to Digital (ADC) based processing system that used an interpolation algorithm [9] to compute the phase differences. This algorithm was implemented in sofware [7,17]. The signals were first down-converted from the optical frequencies to the heterodyne frequencies (40 MHz) and then to the intermediate frequency (1 MHz) for its digitization and later post-processing.

With the advances in technology the off-line processing system of the TJ-II IR interferometer was replaced by a system based on FPGAs and fast ADCs. This system is depicted in Figure 3. First the signals were digitized using high speed ADCs. The digitized data was fed into a pre-processing stage where basically the signals were zero padded, interpolated and filtered, the phase differences were then demodulated using the interpolation algorithm described in [15–17] and in a post-processing stage the demodulated phase differences were filtered and integrated, and finally the line-integrated electron density was calculated according to Eq. 11.

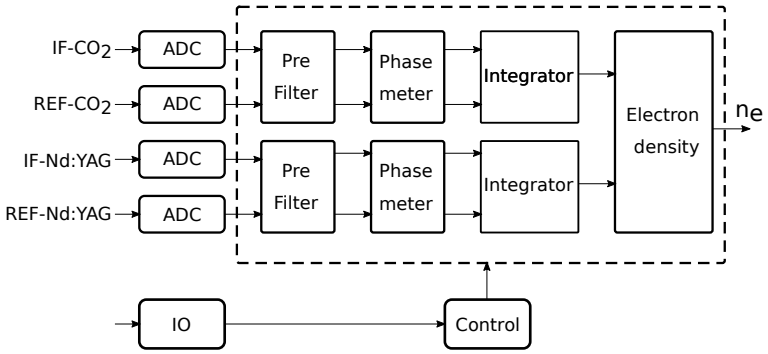

Figure 3. Architecture of the FPGA based processing system.

3. Discussion

Before measuring the electron plasma density, the performance of the interferometer and the FPGA-based measuring system have been tested under static conditions, without currents on the

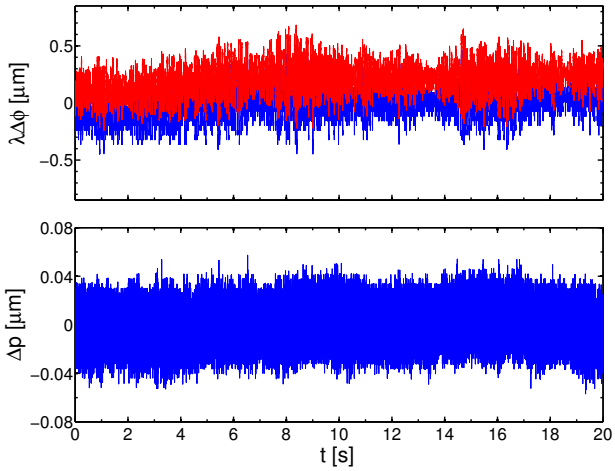

Figure 4. Optical paths of CO_2 and Nd:YAG, (a) for static conditions, both traces follow the mechanical vibrations. In (b) both traces have been subtracted to obtain the compensated optical path length that under plasma conditions would be proportional to the line-integrated electron density.

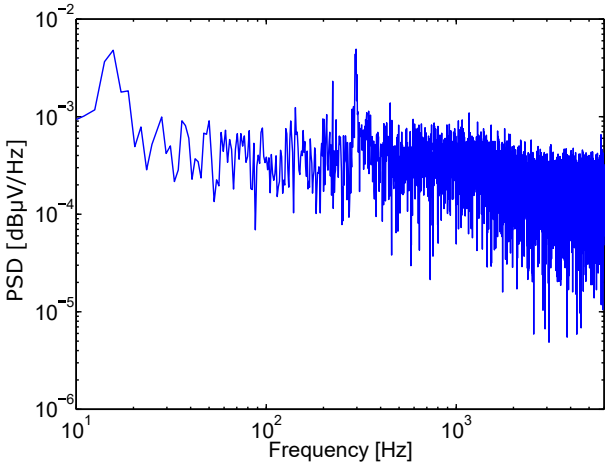

Figure 5. Spectrum of the compensated optical path length signal, from 10 Hz to 6.4 kHz.

TJ-II coils, without heating nor gas puffing in the magnetic fusion device. In Figure 4 (a), the optical path lengths of both the CO_2 and the ND:YAG are illustrated, for the sake of clarity the CO_2 trace has been displaced 0.1 μm, the ripple of both traces is because of mechanical vibrations that affect the interferometer. The compensated signal is obtained after subtracting both optical path lengths, which gives a measure of the error of the interferometer under non-plasma conditions. This issue is shown in Figure 4 for an acquisition of 20 s resulting in an standard deviation of 0.0151 μm and a bandwidth of 6.4 kHz. The final resolution of the compensated optical path length can be improved at the expense of narrowing its bandwidth [15].

Figure 5 shows the Fast Fourier Transform (FFT) of the compensated signal of Figure 4 (b). The spectrum exhibits a $1/f^2$ behavior. The peak located at 295 Hz is generated by a pump rotating at 17700 rpm.

Plasma operation in TJ-II begins with three technical pulses, in the first two no plasma is generated and in the third one typically a plasma of low density appears. In Figure 6 (a), (b) and (c) the first three technical shots of the beginning of an operation day are shown. The currents through the coils are increased in each shot, these currents make the machine to move slightly with respect to the optical table. This movement is measured by the interferometer, in the first technical shot this displacement is

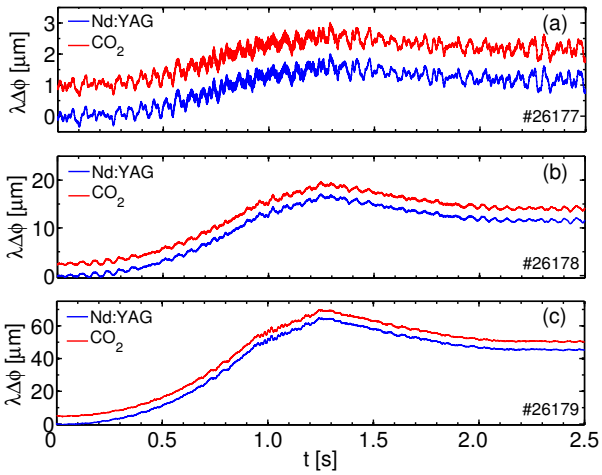

Figure 6. Technical shots acquired during one operation day at the TJ-II Stellarator. Offsets of 1 μm, 2.5 μm and 5 μm have been introduced in the CO_2 traces of correspondent to the first, second and third technical shots, respectively.

in the order of 3 μm, in the second one in the order of 18 μm and finally in the third one in the order of 70 μm.

In Figure 7 the compensated optical path length of technical shot (a) is shown. In this particular case, the error measured as the standard deviation of the compensated optical path length is 0.0157 μm **which is 1/674 of a** CO_2 **fringe** 10.591 μm**.**

These technical shots allow the verification of the behavior of the system before the daily operation in case it is necessary to perform modifications. During the rest of the operation the Torus hall is only opened for short periods of time.

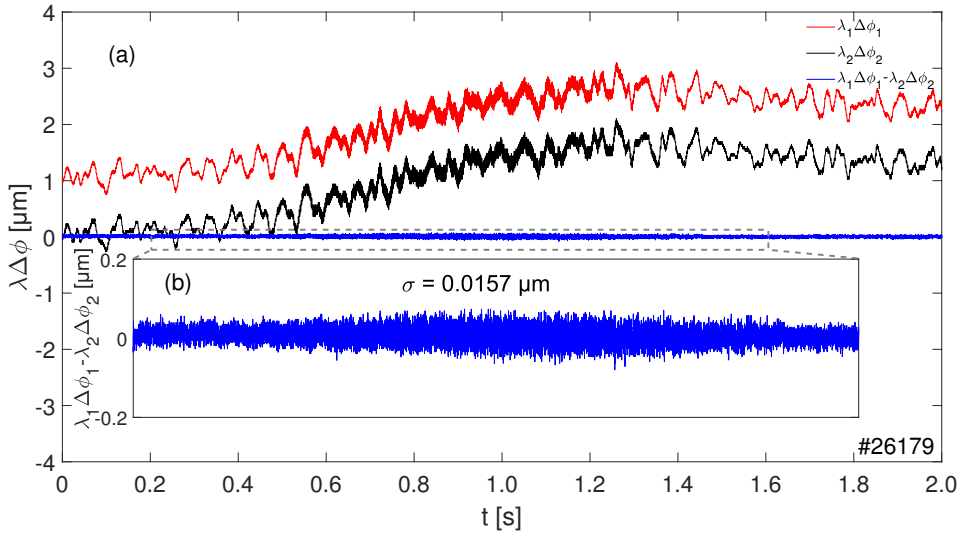

Figure 7. Compensated optical path length for technical shot #26177.

In Figure 8, the measurements of both optical path lengths, CO_2 and Nd:YAG corresponding to shot number #26196, are illustrated. The line-averaged electron density is proportional to the difference between the two traces, as it can be seen in the detail of the figure, this density is calculated applying Eq. 11 where the value of the chord length (integration path across the plasma) is 0.4 m for this particular case.

In Figure 9 the line-integrated electron density for shot number #26196 is shown. The plasma was heated using Electron Cyclotron Resonance Heating (ECRH) and Neutral Beam Injection (NBI), and for

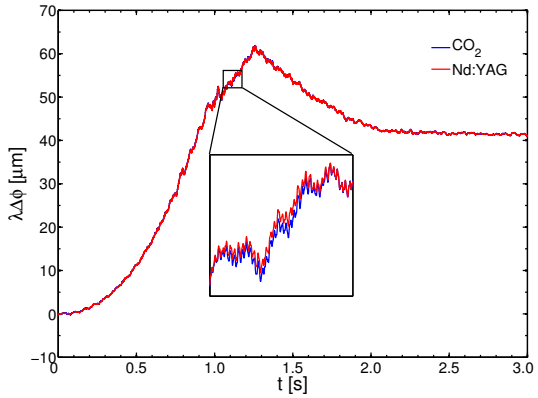

Figure 8. Measurements of both optical path lengths, CO_2 and Nd:YAG for shot #28196. The maximum movement of the TJ-II with respect to optical table is about, 63 μm. As it can be seen in the detail of the figure a gap exists between the two traces from second 1 to about second 1.3, this gap corresponds to the line-integrated plasma electron density.

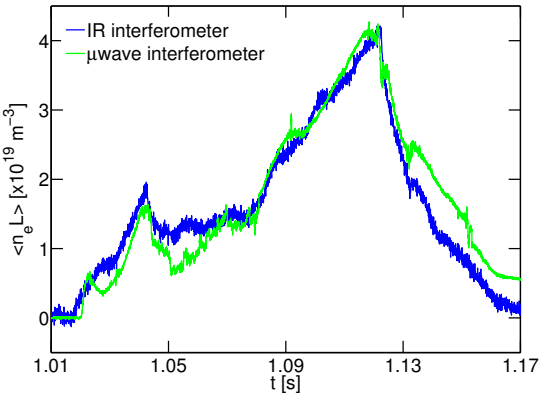

Figure 9. Shot number 26196. The blue line corresponds to the measurement performed with the infrared interferometer and the online FPGA-based processing system. As it can be seen in the figure a difference between the two traces exists, this is because there are uncorrected fringe jumps in the μwave interferometer signal, green line.

comparison, both measures the one taken from the μwave interferometer [18] and the IR interferometer are shown. The blue trace is the measure obtained with the IR interferometer while the green one corresponds to the TJ-II μwave interferometer ($\lambda = 2.14$ mm). The latter uses an analog phase measuring system based on In/Quadrature (I/Q) demodulation. The density is calculated off-line after sampling and unwrapping the In-Phase Quadrature component. For high densities, Figure 9 the line-integrated density is difficult to reconstruct because the plasma is near the cutoff density and starts to become reflective for the μwave radiation. **Under these circumstances the unwrapping algorithm is not able to correct all the fringe jumps, as it can be seen in the $3 \cdot 10^{18}\mathrm{m}^{-3}$ pedestal at the end of the line-averaged electron density trace of Figure 10.**

As explained in Section 1 for high plasma densities the infrared interferometer is more reliable on the other hand, the infrared interferometer is more sensitive to mechanical vibrations and low frequency drifts. Furthermore, as the electron density provided by the IR-interferometer does not suffer of fringe jumps, it can be used **for the measurement of the line-averaged electron density when the μwave interferometer cannot provide reliable results (high densities).**

The next three plots, Figure 11, Figure 12 and Figure 13 correspond to shots, #26334, #26335 and #26336 in which the plasmas have been generated using both ECRH and NBI heating.

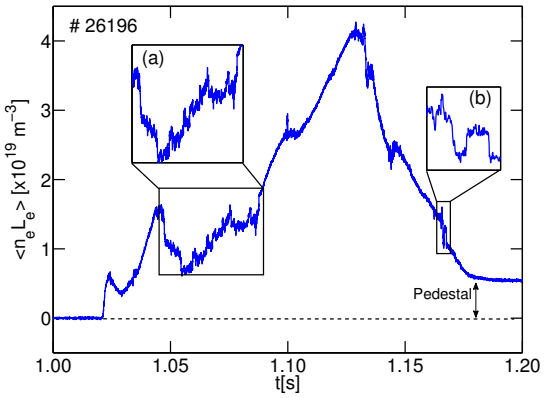

Figure 10. Detail of the measurement performed by the microwave interferometer for shot number 26196. In the details of the figure, (a) and (b) several fringe jumps are shown. The result is a final artificial pedestal at the end of the discharge.

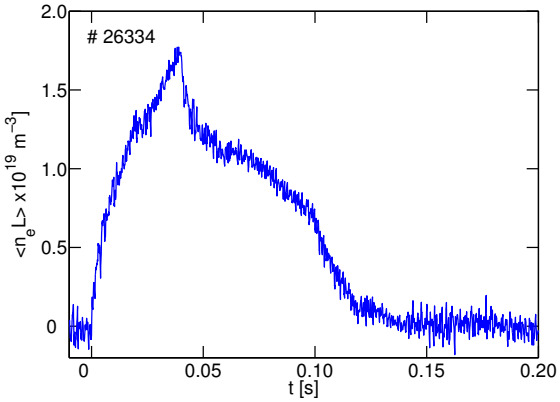

Figure 11. Shot number # 26334.

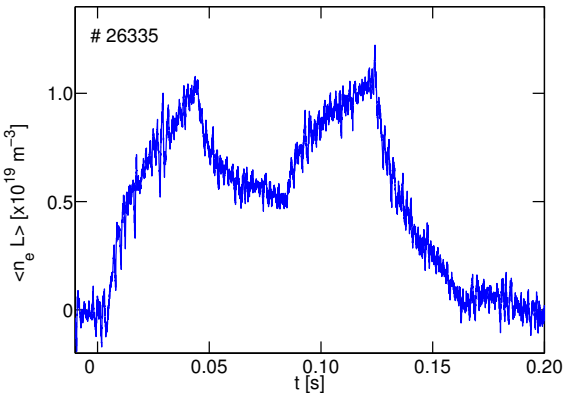

Figure 12. Shot number # 26335.

The error in the measurements is better than $5 \cdot 10^{17}$ m^{-3} and furthermore the measurements are free of fringe jumps due to algorithmic computation, which allows the correction of the μwave interferometer signals for high electron densities. Fringe jumps can appear because of miss-alignment of the beams.

The behavior of the phase meter as it is implemented, when no probing interference signals are detected, is like a free running counter. This happens when the interference signals are lost. When the counters reach their maximum value, the output signal is wrapped. A transient loss of the interference

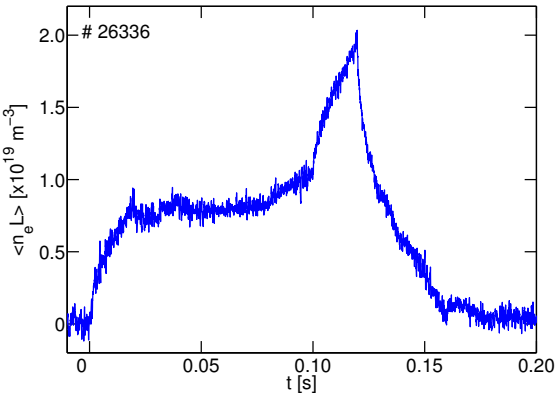

Figure 13. Shot number # 26336.

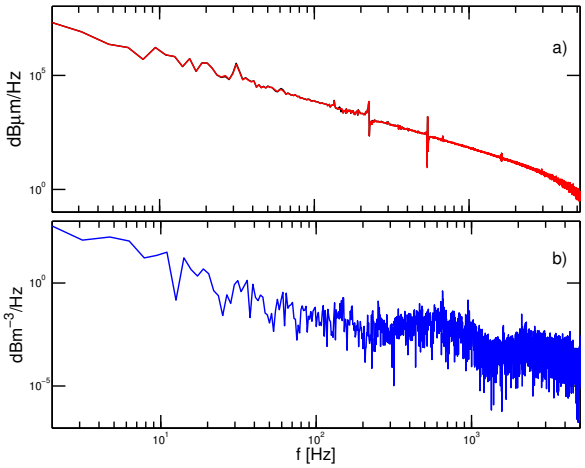

Figure 14. Spectrum of the density signal correspondent to shot number # 26334. Several spectral peaks are observed centered in the frequencies, $\sim$ 75 Hz, 300 Hz, 450 Hz and 520 Hz. Having the three last their origin in several turbo-pumps operating in TJ-II.

signals causes the apparition of fringe jumps in the measure. In Figure 15 these effects are shown, the blue line corresponds to the CO_2 trace in which a transient lose of the interference signal occurs, for instance at second 1.07. The Nd:YAG signal is almost completely lost when the machine begins to move. The phase measuring system continuously loses fringes, as no interference signal is present in the inputs of the ADCs. The effect is caused when the beams are tilt because of the movement of the machine and the beams move out of the detection area. This effect is caused because of miss alignment of the interferometer and it is more severe the longer the geometrical paths of the interferometer are and the narrower the width of the spots are.

4. Conclusions

The line-integrated measurement system of TJ-II has been tested during normal operation of the TJ-II device. Three types of measurements have been performed, without plasma and magnetic fields, with magnetic fields (technical shots), and with magnetic fields and plasma. The measurements of infrared interferometer have been compared with those of the μwave one, showing no fringe jumps in the first while in the second it is almost impossible to reconstruct the density profile for high gradients. However, the measures performed with the infrared interferometer are more sensitive to vibrations and low frequency drifts as it could be expected from Eq. 11. Also, it has been shown that when the interference signal is lost fringe jumps appear in the measurements and therefore it is almost impossible to calculate the line-electron density.

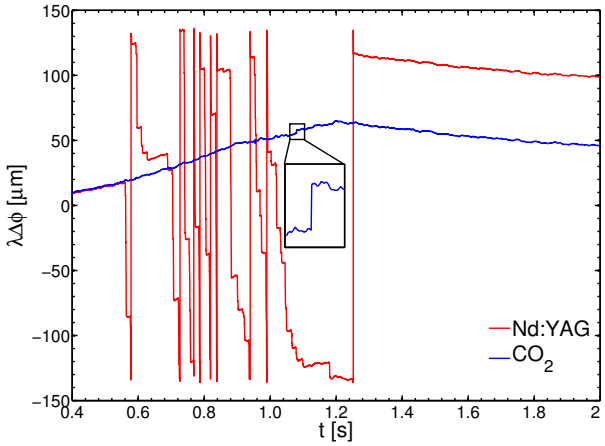

Figure 15. The probing Nd:YAG interference is lost which originates jumps proportional to the integer bit-width (dynamic range) of the output optical path length subtractor. The CO_2 interference signal is also transiently lost, as it can be seen in the detail of the figure.

Under static conditions resolutions in the order of $10^{-2}\mu$m can be obtained. With plasma and mechanical movements of the TJ-II the error is slightly worse, in the order of 1/400 of a CO_2 fringe which is about $3 \cdot 10^{-2}\mu$m or in terms of line-averaged electron density of $5 \cdot 10^{-17}$ m^{-3}. It should be highlighted that the calculation of the line-averaged electron density is performed online using an FPGA and high speed Analog to Digital Converters.

References

1. Wesson, J. *Tokamaks*; Oxford university press, 2004.
2. Hartmann, D.A. Stellarators. *Fusion Science and Technology* **2004**, *45*.
3. Gurnett, D.A.; Bhattacharjee, A. *Introduction to Plasma Physics, With Space and Laboratory Applications*; Cambridge University Press, 2005.
4. Appleton, E.V. Wireless studies of the ionosphere. *I.E.E* **1932**, *71*, 257–265.
5. Hutchinson, I.H. *Principles of plasma diagnostics*; Cambridge University Press, 1990.
6. Hartfuss, H.J.; Geist, T.; Hirsch, M. Heterodyne methods in millimetre wave plasma diagnostics with applications to ECE, interferometry and reflectometry. *Plasma Physics and Controlled Fusion* **1997**, *39*, 1693.
7. Zubarev, P.V.; Khilchenko, A.D. Precision Phase Discriminator for the Heterodyne Interferometric Plasma-Density Measurement Technique. *Instruments and Experimental Techniques* **2003**, *46*, 171–176. 10.1023/A:1023661531511.
8. Sevillano, E.; Irby, J.H.; Lipschultz, B.; Marmar, E.S.; Post, R.S. Multichord interferometer for edge density profiles in Alcator C-Mod (abstract). *Review of Scientific Instruments* **1988**, *59*, 1591–1591. doi:10.1063/1.1140154.
9. Sanchez, M.; Sanchez, J.; Estrada, T.; Sanchez, E.; Acedo, P.; Lamela, H. High resolution CO[sub 2] interferometry on the TJ-II stellarator by using an ADC-based phase meter. *Review of Scientific Instruments* **2004**, *75*, 3414–3416. doi:10.1063/1.1786638.
10. Kawahata, K.; Ejiri, A.; Tanaka, K.; Ito, Y.; Okajima, S. Design and construction of a far infrared laser interferometer for the LHD. *Fusion Engineering and Design* **1997**, *34-35*, 393 – 397. Fusion Plasma Diagnostics, doi:DOI: 10.1016/S0920-3796(96)00608-4.
11. Jacobson, A.R.; Call, D.L. Novel interferometer for the measurement of plasma density. *Review of Scientific Instruments* **1978**, *49*, 318–320. doi:10.1063/1.1135399.
12. et al., K.B. Real-time dispersion interferometry for density feedback in fusion devices. *Journal of Instrumentation* **2018**, *13*, P09002.
13. Dreier, P.K.M.H.T.B.A.D.H.; Hartfuss, H.J. Design of multichannel laser interferometry for W7-X. *Rev. Sci. Instrum.* **2006**, *77*, 10F128.

14. Ohtsuka, Y.; Sasaki, I. Laser Heterodyne Measurement of Small Arbitrary Displacements. *Optics Comunications* **1974**, *10*, 362–365.
15. Nieto-Taladriz, L.E.M.S.J.A.L.O.; Sánchez, J. Continuous plasma density measurement in TJ-II infrared interferometer-Advanced signal processing based on FPGAs. *Fusion Engineering and Design* **2010**. doi:doi:10.1016/j.fusengdes.2010.03.036.
16. Fernández, L.E.M.S.J.S.P.K.M.H.J.A.L.A.; Nieto-Taladriz, O. Continous phase measurement in the W7-X IR-interferometer by means of an FPGA and high speed ADCs. *Fusion Science and Technology* **2010**.
17. Esteban, L.; Sánchez, M.; López, J.A.; Nieto-Taladriz, O.; Kornejew, P.; Hirsch, M. Development of efficient FPGA-based multi channel phase meters for IR interferometers. *IEEE Transactions on Nuclear Science* **2011**, *58(4)*, 1562 – 1569.
18. Manso, T.E.J.S.B.V.M.L.C.A.S.M.E.; Zhuravlev, V. Density profile measurements by AM reflectometry in TJ-II. *Plasma Phys Control Fusion* **2001**, *43*, 1535–1545.